Earliest version, intended for internal use. Has target dimensions tables that later versions do not.

Long version

UCRL-ID- 110142

Has target dimensions

VISAR Wave Profile Study of Bristol Rock

David Erskine

Physics Department/ H-Division
Lawrence Livermore National Laboratory
University of California
Livermore, CA 94551

March 1992

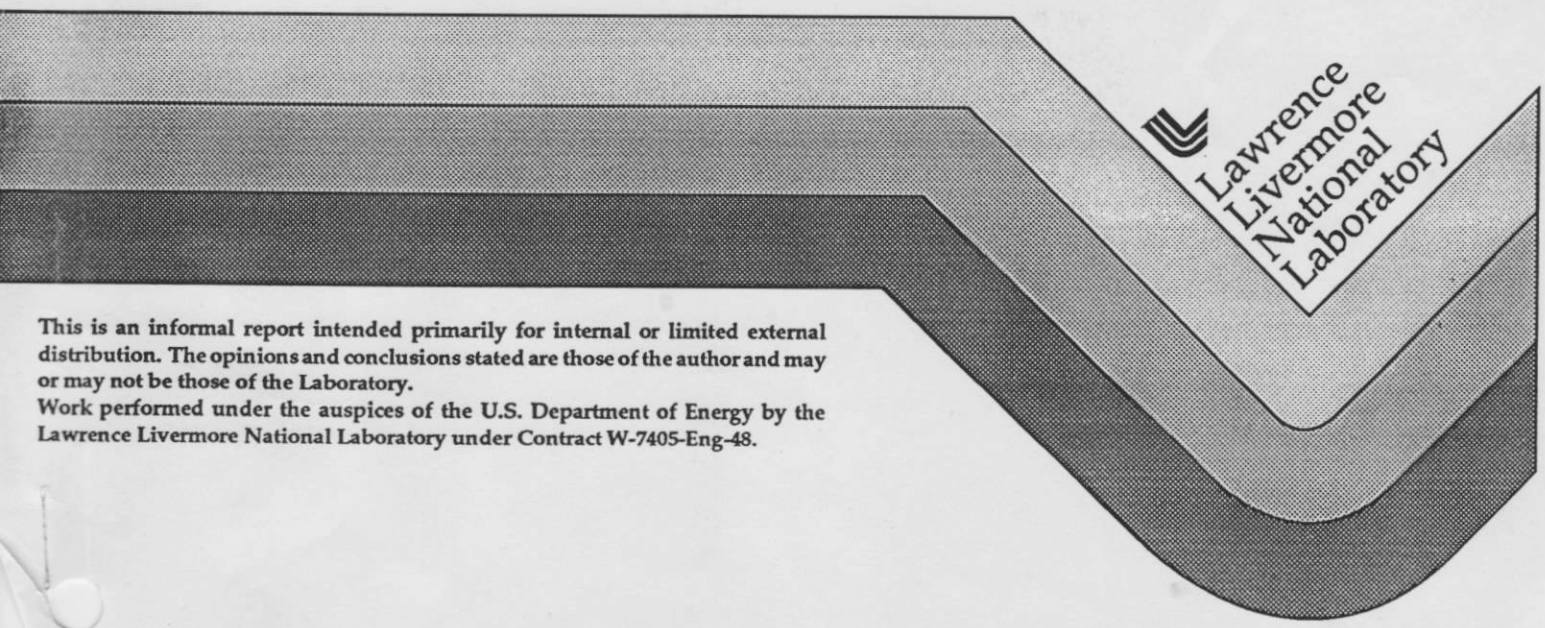

Work performed under the auspices of the U.S. Department of Energy by the Lawrence Livermore National Laboratory under Contract W-7405-Eng-48.

VISAR Wave Profile Study of Bristol Rock

Dave Erskine

H-Division

Lawrence Livermore National Laboratory

Livermore, CA 94550

Abstract

Hugoniot and release equation-of-state data are measured on samples from the U4AV emplacement hole at the Nevada Test Site, used for the Bristol shot. Wave profiles were measured using a VISAR velocimeter and a target with forward-geometry. The transit time of a shock through the sample provides the Hugoniot information. The shape of the wave profile indicates the arrival of a release wave, providing the sound speed in shocked rock and equation-of-state properties in release. The shape of the leading edge of the profile provides information on the compressive dynamics of the shock phenomena in the rock, such as pore crushing or phase transformations. The same rock was tested in a water saturated and semi-dry state. Hydration of the rock increases the Hugoniot and sound speed. The Hugoniot of this rock in a water saturated state is close to that measured by M. Furnish of SNLA on similar rock. The U_s-U_p relation is U_s=2.29 + 1.263 U_p for $1<U_p<2.6$ km/s and U_s=2.04 + 1.408 U_p for $2.6<U_p<5.6$ km/s.

Introduction

In November 1991 the Bristol shot occurred at the Nevada Test Site. One purpose of this shot was a test of the ability to calculate its yield using the CORRTEX method. The success of the method depends on accurately modeling the shock wave properties of the rock surrounding the nuclear device. Both the Hugoniot and release wave properties are needed. Because the character of rock can vary significantly from location to location, it is best to determine the shock properties of the rock at the particular emplacement hole and depth of the device, and to preserve the hydration of the samples to reproduce in situ conditions as much as possible.

To this end, we undertook a series of experiments on a two-stage gas gun using a VISAR velocitometer as a diagnostic on samples of rock taken from the U4AV emplacement hole. These experiments consisted of generating a planar shock wave by impact with a flat projectile. The shock wave transits the specimen and a mass velocity wave profile is measured as the shock emerges from the rear of the sample. The transit time of the shock across the sample yields the shock velocity and a Hugoniot point. The shape of the wave profile showing the arrival of a rarefaction wave yields the release wave properties.

We completed two series of Hugoniot measurements on the same rock. In series-I we attempted to preserve the original hydration of the samples by coating them with a sealant. However some water loss did occur. In series-II the rock was shot in a rehydrated state close to its original density. Thus in addition to determining the shock properties of in situ rock, we have measured its dependence on hydration.

We used a forward-geometry target design to obtained the wave profiles, instead of a reverse geometry employed by researchers at SNLA[1] studying similar rock. The advantage of the reverse geometry lies in a superior measurement of the release properties of the sample, whereas the forward geometry makes a superior measurement of the shock speed and the detection of phase transitions and other anomalous compressive behavior. Because of additional cost advantages, we decided to employ the forward geometry technique.

Samples

The rock samples were taken from cores drilled into the wall of the emplacement hole at nine specified depths from 1100 ft to 1500 ft. After removal from the coring tool the samples were immediately sealed in aluminum foil and wax to preserve their water content. Portions from each depth were sent to TerraTek Inc. for analysis[2]. The results of their analysis are listed in Table A.I in the Appendix.

There was significant variation of the character of the rock with depth in terms of friability and grain size. We chose to study 1410 ft. rock for the bulk of the shots because it was competent, its grain size was uniformly small, and it was in the vicinity of the device working-point depth (1500 ft.). The 1500 ft. rock was not preferred, because although it was slightly more competent than the 1410 ft., it possessed an occasional large (~3 mm) grain which could disrupt the fidelity of the measured wave profile. The target sample thickness was 7 mm. For the 1410 ft. rock the average grain size was ~ 1 mm.

The in situ density of the 1410, 1490 and 1500 ft. rock was determined by the Archimedes method. A thin plastic bag prevented water from leaving or entering the sample during this measurement. The results were 1.87, 1.74 and 1.91 gm/cm^3 for 1500, 1490 and 1410 ft. elevations. Since the rock specimen was large, and the measurement was made immediately after unsealing from the wax/aluminum foil, these density values are accurate determinations of the average density of the rock prior to machining and handling.

In order to preserve the water content, the rocks were spray-painted with an epoxy sealer. Sealer was reapplied after the rocks were machined into disks for incorporation into targets. In spite of the sealer, some water loss did occur. The density of the 1410 ft. rock samples immediately before incorporation into the targets was 10% less than its original value (~1.7 vs 1.9 gm/cm^3). Shot series-I used this rock in this semi-dry state. We use the term "semi-dry" to distinguish it from "dry". The latter would be the case if all the water were baked out. According to Table A.I, the dry density of the 1410 ft. rock is 20% below the original density.

Because we were concerned that the measured shock data of the semi-dry rock might not be representative of in situ rock, we undertook a second shot

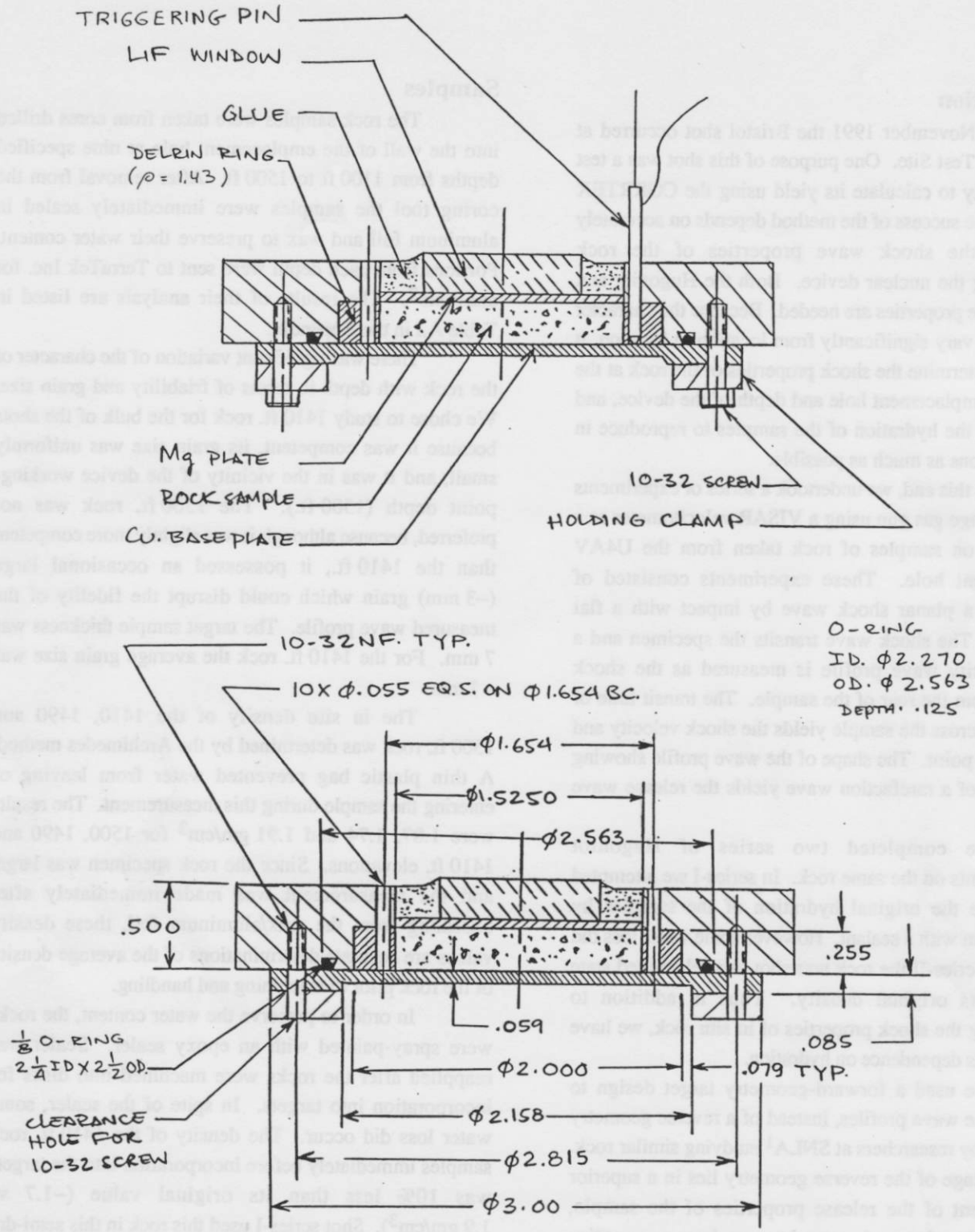

Fig. 1. **Target design for water-saturated rocks,** using the 2 inch gun barrel. For the 1.125 inch barrel the sample diameter was 19 mm and the other horizontal dimensions were similarly reduced. The flyer impacts from below. Dimensions shown are in inches. The target design for the semi-dry shots is similar, but without the baseplate.

series (II) using rehydrated rock. Soaking the rock in water increased its density from ~1.7 to 1.87 gm/cm^3, which is very near its 1.91 gm/cm^3 original value. Only the 1410 ft. rock was tested in series-II.

Although the Hugoniot information from shot series-I is not as representative of rock immediately surrounding the device due to the different hydration state, this data is still useful. Comparison of the two series' data indicates the sensitivity of the Hugoniot on water content. This facilitates estimating the shock properties of other rock at the emplacement hole that may be less than water saturated.

Experimental Technique

Target Design

The target design for the series-II experiments using water saturated samples is shown in Fig. 1. The target design for series-I experiments is similar, but without the baseplate and O-ring. A 2" diameter gun barrel was used for all shots except the highest pressure shots R_{wx} and R_{yz}. For the latter the 1.125" barrel was used to attain the required impactor velocity, and the horizontal dimensions of the target were accordingly reduced. Tables A.II - A.V give the thicknesses and densities of the component layers for the wet and semi-dry rock target designs.

In the target the water saturated rock is contained in the Delron ring between a Cu baseplate and the Mg backplate. An O-ring provides a seal. Behind the Mg is a LiF window, which allows the VISAR laser beam to probe the velocity of the Mg while avoiding a free surface. The Delron has a shock impedance similar to the rock. This prevents a shock in the aluminum from running around and ahead of the shock in the sample. The Delron also reduces the amplitude of a side release generated at the front corner of the sample. The aspect ratio of the sample (5.5:1) is great enough to ensure that the side release wave will not interfere with the measurement of the wave profile at the center of the Mg/LiF interface.

Wave paths

These targets are of the forward-geometry type, where both the shock and release waves travel forward through the sample toward the LiF window. This is distinguished from the reverse-geometry, where the sample is contained in the impactor and the shock moves backwards through it, away from the window.

Figure 2 is a distance-time plot of the important wave paths. The shock generated by impact of the projectile travels forward through the baseplate, rock, Mg backplate, and into the LiF window. Electrical shorting pins flush with the baseplate/sample interface provide a start time of the shock arrival. The motion of the Mg/LiF interface is measured with the VISAR velocitometer. After accounting for the transit time of the shock across the Mg, the time of arrival of the shock at the interface gives the shock speed (U_s) across the rock, yielding the Hugoniot information. A second shock travels backwards across the Cu impactor, reflects from the rear of the Cu, and travels forward as a release wave. The time of arrival of this release wave yields the sound speed in the rock in its shocked state.

The purpose of the Mg backplate is to minimize the thickness of the rock which is double-shocked by reflection of the incident shock off the LiF window. In this way, the release wave travels virtually only through rock that is singly-shocked, as illustrated in Fig. 2. Secondly, it protects the hygroscopic LiF from moisture in the rock. The thicknesses of the Mg layer and Cu flyer are designed so that the release wave transits the rock before the reflection from the Mg/LiF interface can interfere. There is also an unavoidable reflection from the rock/Mg interface, but this is relatively weak since the densities of Mg and rock are similar. For example, for shot R_i the rock/Mg reflection increases the pressure 18%. In a target without the Mg layer the rock/LiF reflection would increase the pressure 50%.

Forward versus reverse geometry.

We decided to use forward-geometry targets over reverse-geometry for several reasons. 1) In the reverse geometry there is a danger that the sample will fracture when accelerated in the launch of the impactor. 2) Expensive large LiF crystals are required in the reverse-geometry. 3) The forward geometry allows samples to be twice as thick for a given diameter before side release waves interfere with the measurement. Since the grain size of these samples is significant, it was important to maximize the sample thickness as much as possible. 4) The U_s-U_p data point is determined from the arrival time of the shocks instead of the amplitude of the VISAR

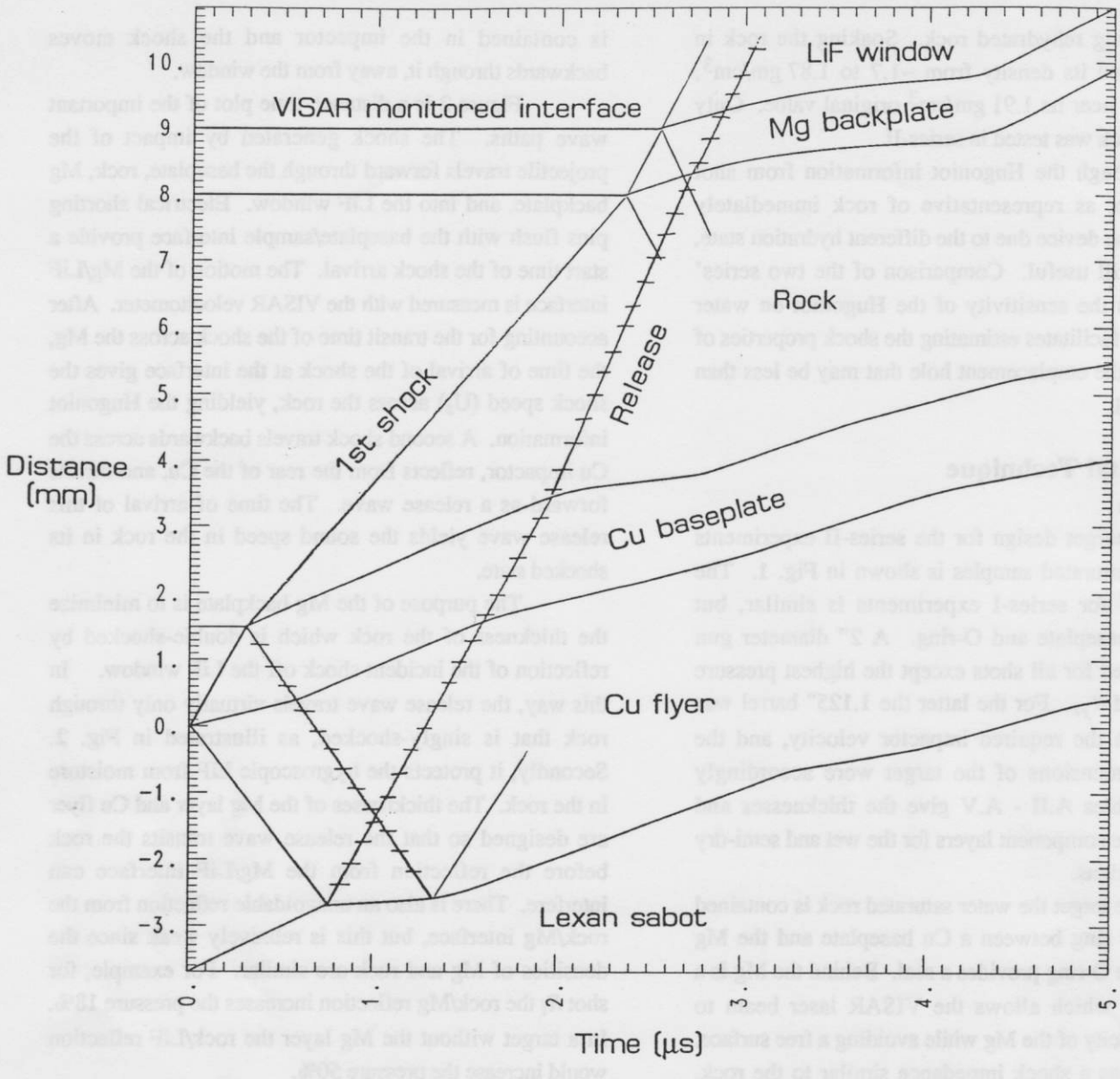

Fig. 2. Distance-time diagram of target impact. Rarefaction waves are indicated by crossed lines. The VISAR measures the wave profile at the Mg/LiF interface.

signals. With the VISAR, amplitude accuracy is not as great as the temporal accuracy of shock transit time. 5) In the forward-geometry, the front of the wave profile yields compressive behavior of the rock such as phase transitions, strength effects and the effect of pore crushing.

On the other hand, the forward geometry presents an inferior measurement of the release wave properties of the rock. The shape of the release portion of the wave profile is complicated by reflections from the Mg layer. Also, the release wave does not descend to as low of a pressure as in the reverse geometry when a low density foam is used behind the sample-impactor.

VISAR velocitometer diagnostic

The velocity history of the Mg/LiF interface is measured by the VISAR velocitometer. The VISAR works by measuring the doppler shift of the reflected light. A lens mounted behind the LiF window focuses the illuminating beam to a ~1 mm spot at the center of the LiF/Mg interface and collects the reflected light. This is sent to an interferometer which resolves the wavelength shift into fringes. Our interferometer is a push-pull design similar to that described in Ref. 3. The fringe shift is proportional to the velocity, with a proportionality constant of 453 m/s per fringe±1%. The fringe shift is detected by photomultiplier tubes recorded by a digitizing oscilloscope with 1 ns sampling rate. The overall time response of the velocitometer system is about 1.5 ns. The absolute velocity error is about 1%, determined by the uncertainty of fringe constant. The resolution of the velocity however is much higher.

Data Analysis and Results

The shock speed in the rock is determined from the shock arrival time in the wave profile record, subtracting the calculated transit time of the shock across the Mg layer. The latter is found iteratively. The mass velocity of the shocked rock (U_p) is found from shock-impedance matching using U_s, the flyer velocity and the Cu Hugoniot. Since we have nanosecond resolution in determining the arrival times, the uncertainty in U_s and U_p is <1%.

The U_s-U_p data for both series is shown in Fig. 3 and tabulated in Tables I and II. Coefficients for best-fit line segments passing through groups of points are indicated. The Hugoniot of the wet rock lies above that of the semi-dry rock. Ultrasonic measurements of the

Table I. Shot data for rehydrated samples. U_s and U_p are experimentally determined shock and mass velocities in 1410 ft. rock sample. P and ρ/ρ_0 are the shock pressure and relative compression.

shot	flyer vel (km/s)	U_p(km/s)	U_s (km/s)	P (kbar)	ρ/ρ_0
R_h	1.390	1.174±0.2%	3.783±0.6%	81.9	1.45
R_i	2.323	1.915±0.2%	4.689±0.7%	165	1.69
R_j	3.185	2.574±0.2%	5.553±0.6%	265	1.86
R_{yz}	5.269	4.078±0.6%	7.854±0.8%%	610	2.08
R_{wx}	7.435	5.633±0.6%	9.966±0.8%	1068	2.30

Table II. Shot data for semi–dry samples. U_s and U_p are experimentally determined shock and mass velocities in rock sample. P and ρ/ρ_0 are the shock pressure and relative compression. R_g is 1500 ft. rock; all other are 1410 ft.

shot	flyer vel (km/s)	U_p(km/s)	U_s (km/s)	P (kbar)	ρ/ρ_0
R_e	1.354	1.182±0.2%	3.178±0.25%	63	1.59
R_d	1.774	1.524±0.25%	3.695±0.4%	94	1.70
R_b	2.722	2.277±0.3%	4.628±0.5%	182	1.97
R_g (1500 ft.)	2.706	2.258±0.3%	4.583±0.5%	182	1.97
R_c	3.170	2.648±0.3%	4.840±0.6%	220	2.21

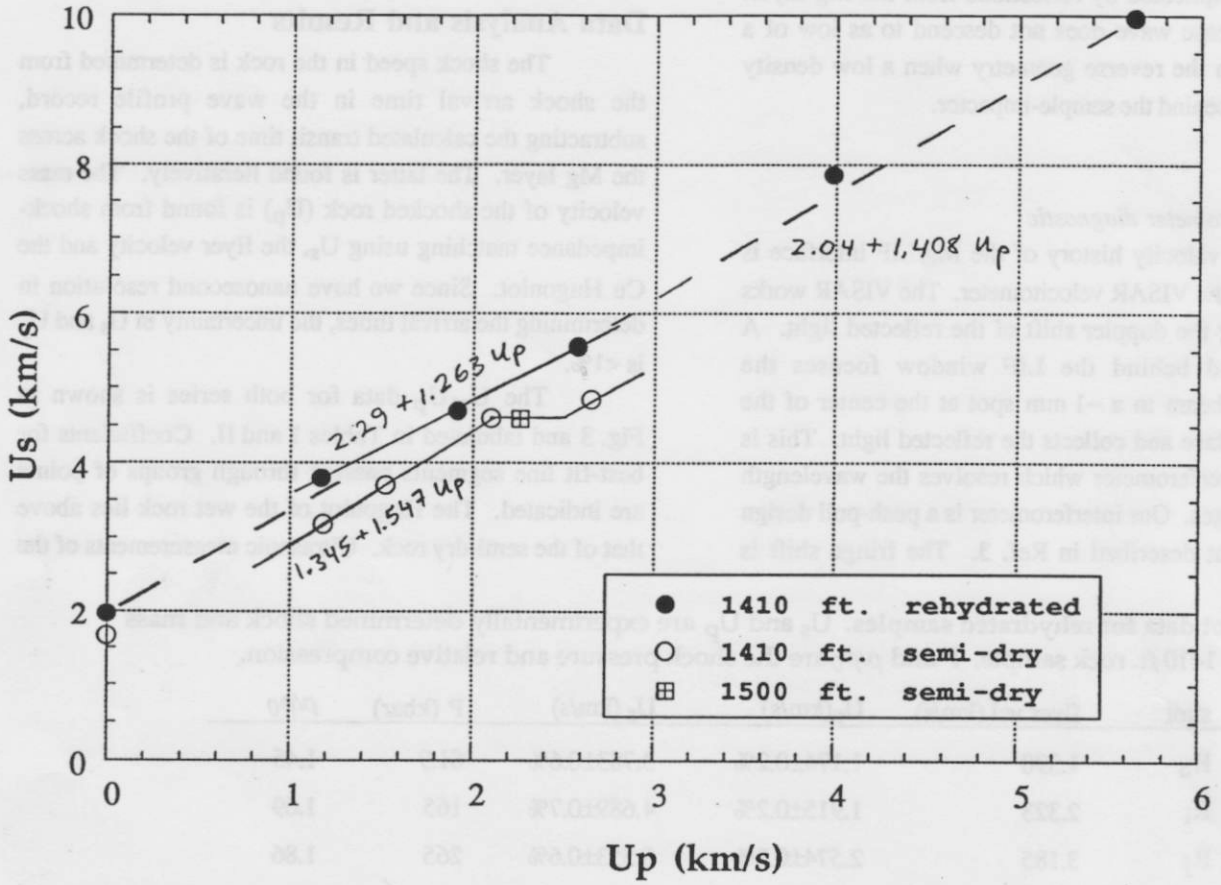

Fig. 3. **U_s - U_p plot for rehydrated and semi-dry tuff.** The U_p=0 data are measured ultrasonic bulk sound speeds for 1410 ft. rock in its semi-dry and rehydrated states.

bulk sound velocity C_b are indicated at U_p=0. They show a small shift due to the rehydration of the rock. (Details of the ultrasonic test are described in the Appendix).

With the wet rock, the data deviates from a straight line with a slight S-shape. Because the uncertainty in U_s is <1%, we believe this is genuine. In Fig. 4 our wet-rock data is compared with data on NTS tuff measured by M. Furnish[1]. A similar S-shape is seen in his data. Except for our lowest pressure shot R_h, all of our points agree very well with his.

For the semi-dry rock the three points highest in U_p show a softening of the Hugoniot. A phase transition would show a similar effect. As discussed below, the wave profile for shot R_b also suggests a weak phase transition at U_p~2.1. The datum of the 1500 ft. elevation rock shot, R_g, is in close agreement with its companion 1410 ft. shot, R_b.

Series-II wave profiles

The measured and calculated wave profiles for the three lowest pressure shots of the wet rock are shown in Fig. 5. The complex dynamics of the compression of tuff is manifested in the front of the measured wave profiles. For example in shot R_h, the rise during the initial 70 ns may be due to the crushing of pores, which produces a large effective thickness for the shock front. The thickness of the front is $\Delta t\ U_s$ or 0.26 mm. This is consistent with a grain or pore size.

The fluctuations in the signal are not instrument noise but are actual variations in the velocity, most likely due to the graininess of the sample. (The instrument noise is ~0.5 %). The use of a finite sample to model bulk rock behavior is only valid if the grain size is sufficiently smaller than the sample thickness so that an averaging process occurs in the propagation of the wave. In the case of 1410 ft. rock the average grain size was ~ 1 mm, compared to the sample thickness of 7 mm. An occasional larger grain could explain irregularities in the measured wave profiles. The laser spot of ~1 mm is comparable to the size of one grain. However, the 1 mm Mg layer smooths out the profile somewhat.

The calculated profiles in Fig. 5 were computed from target parameters listed in Tables A.II and A.III, a constant gruneisen gamma of zero, and the best fit U_s-U_p relation through the three data: $U_s = 2.29 + 1.263\ U_p$. The latter was derived from the arrival time of the shock. Note that the arrival time and the amplitude of the profile are two independent determinations of the Hugoniot of the rock. (The arrival time is the more accurate of the two since it is inherently an average over all the grains the shock transits, whereas a single large grain near the end of the transit could disproportionately affect the wave profile shape.) Thus the agreement in the amplitude of the measured and calculated profiles is a measure of the self consistency of the U_s-U_p data.

Comparison of the release arrival time between calculated and measured profiles is done in Fig. 6. The gruneisen gamma does not affect the single shock portion of the profile (t<200 ns), but does affect the height of the step at t~200 ns due to a reflection from the Mg layer. Sam Weir[4] of LLNL used a linearly volume dependent gruneisen gamma to model wave profile data of tuff measured by M. Furnish[1]. The best-fit gamma values to Furnish's data were used to calculate profiles shown in Fig. 6. These values are listed in Table III. Although their extreme negative gamma values cause less agreement in the amplitude of the profile for t>200 ns, they cause good agreement in the arrival of the release wave in the two higher pressure shots. However, in the lowest pressure shot R_h the arrival of the release is much faster than can be explained using a conventional gruneisen gamma model. William Moss[5] suggests this can be successfully modeled by incorporating material strength into the constituitive model of the rock.

Figure 7 shows measured and calculated wave profiles for the two high pressure shots in the rehydrated rock. The calculated wave profiles use a gruneisen gamma value of +1 and the best fit U_s-U_p line through the two points: U_s=2.32+1.358 U_p. Unfortunately, both shots were hindered by technical problems involving the

Table III. Gruneisen gamma and its slope used in calculated wave profiles for the rehydrated samples. These values are from S. Weir's best fit to M. Furnish's wave profile data on tuff using a gamma which is linearly dependent on volume[4]. V_1/V_0 is the shock to ambient volume ratio.

shot simulated	$\gamma(V_1)$	$V_0(\partial\gamma/\partial V)$	V_1/V_0
R_h	-1.75	25	0.690
R_i	-2	25	0.592
R_j	-1.5	25	0.536

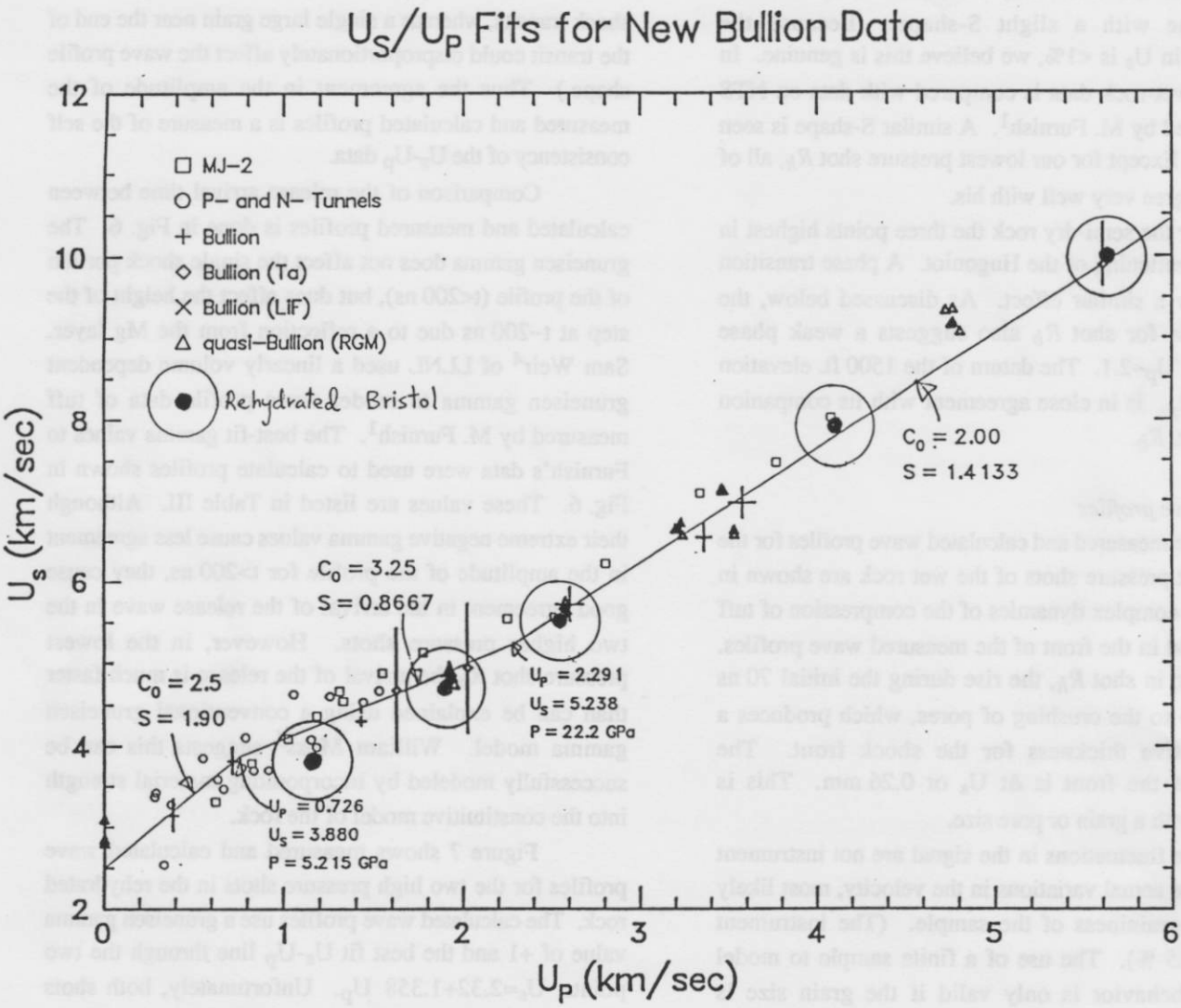

Fig. 4. **U_S-U_P data of NTS tuff by M. Furnish[1] compared to our data,** labeled by the solid circles with halos. Both our tuff and the NTS tuff was wet.

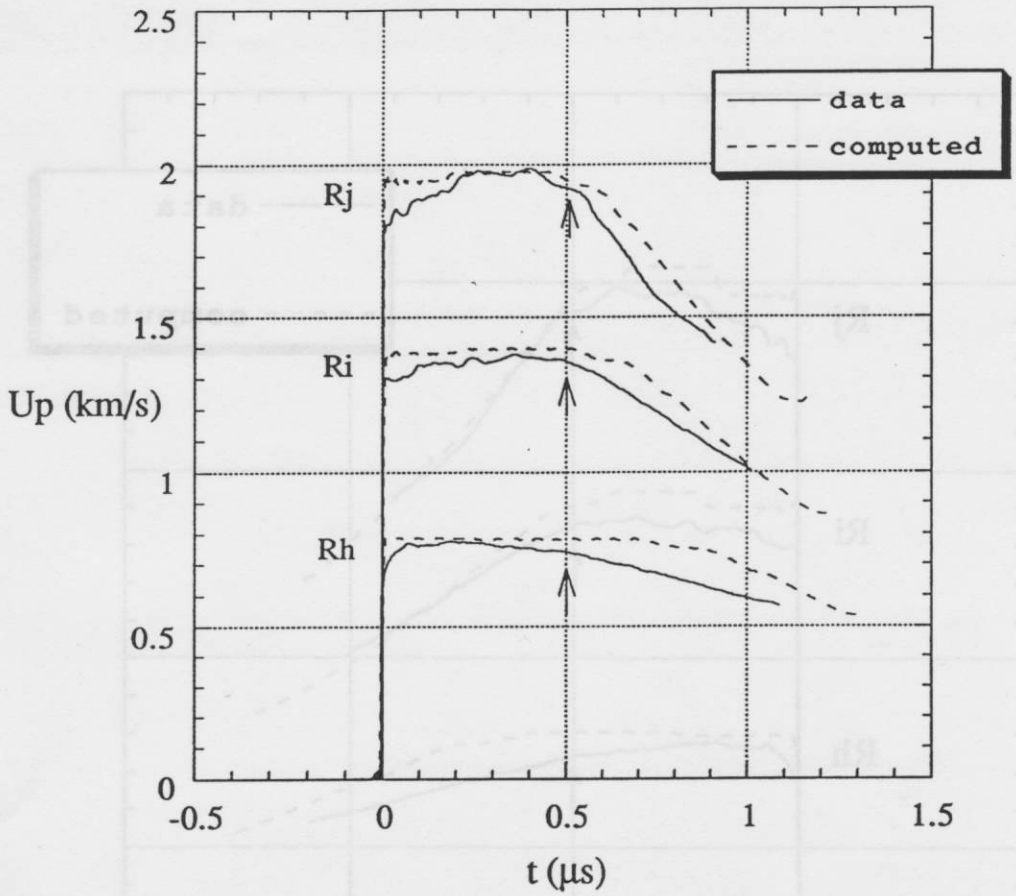

Fig. 5. **Measured and calculated wave profiles for wet rock,** low pressure shots with gruneisen gamma = 0. The material velocity (Up) is measured at the Mg/LiF interface, and time is counted from shock arrival at the interface. The arrows indicate when the release wave was taken to arrive for the sound speed calculation.

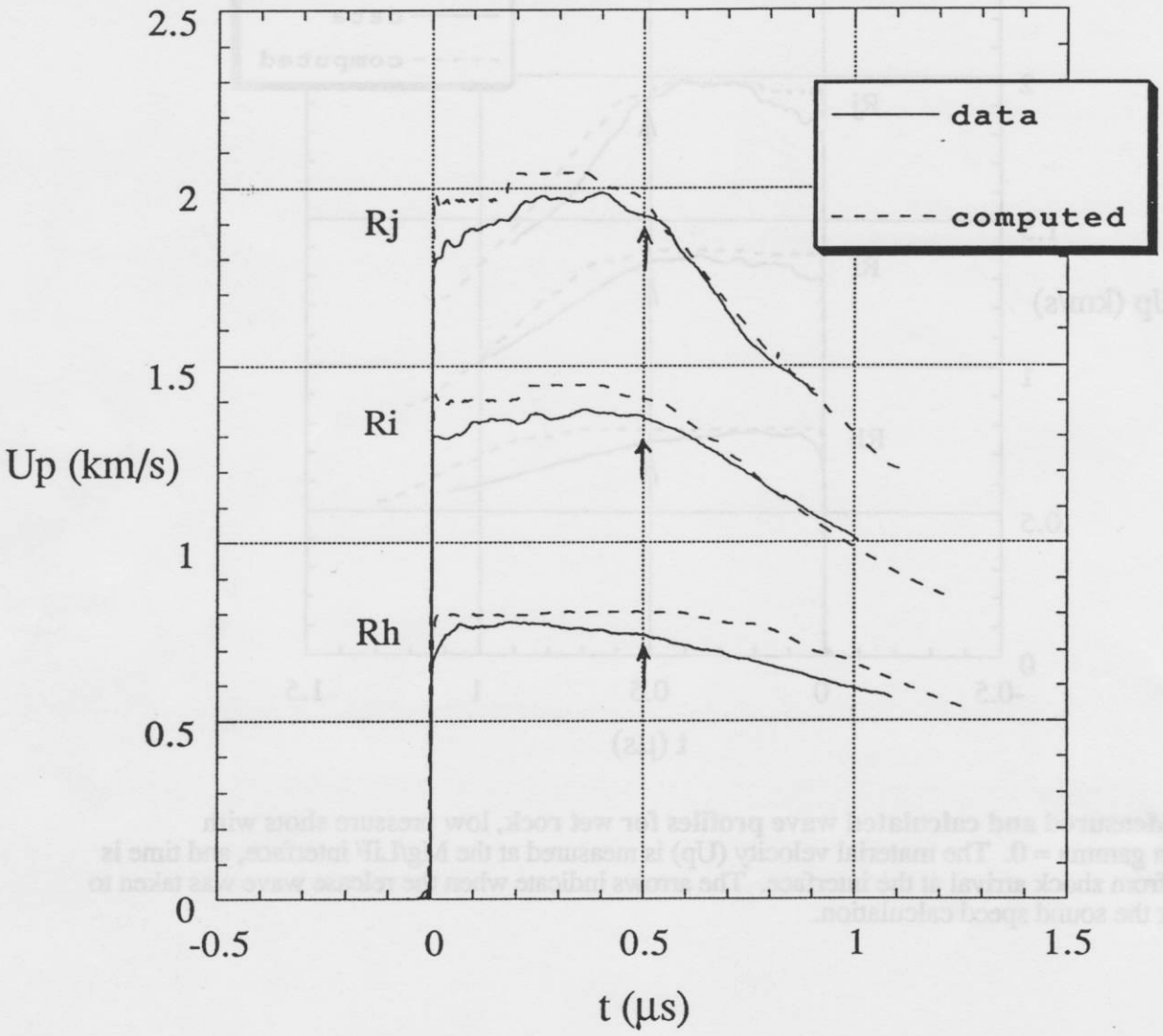

Fig. 6. **Measured and calculated wave profiles for wet rock,** low pressure shots. The calculated waveprofiles use the same parameters as in Fig. 5 except the gruneisen gamma values, listed in Table III, are the best-fit values to Mike Furnish's tuff waveprofiles.

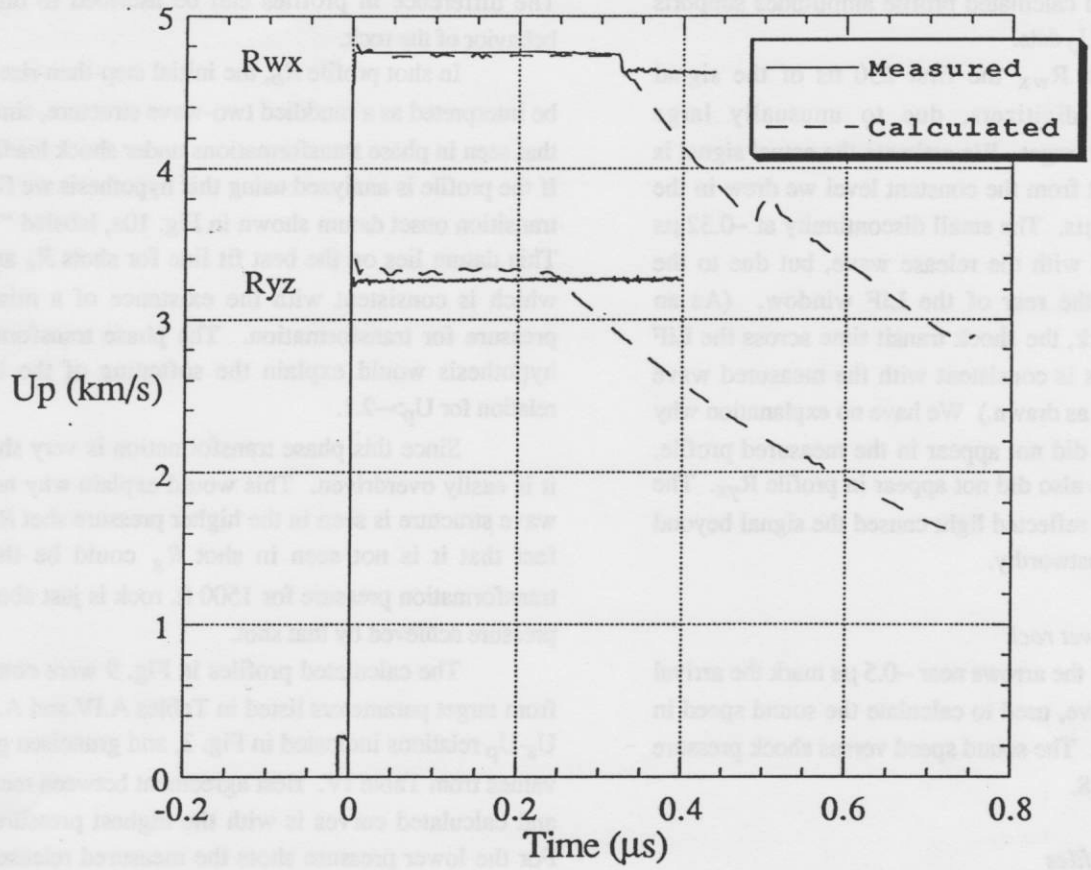

Fig. 7. **Measured and calculated waveprofiles for wet rock,** high pressure shots. Due to unknown reasons the arrival of the release wave does not appear in the measured profiles. (The drop in the data at t=0.32 μs in R_{wx} is not due to the release wave. It is due to the shock reaching the end of the LiF window). However, the U_S-U_P data is accurately obtained from the arrival time of the shock, and the agreement between the calculated and measured waveprofile amplitudes indicates the data is self-consistent.

intensity of the reflected light which partially obscured the shape of the profile. However, the shock arrival time information is unambiguous, and therefore the U_s-U_p data is still perfectly valid. The excellent agreement between the measured and calculated profile amplitudes supports the measured U_s-U_p data.

For shot R_{wx} the first 230 ns of the signal overloaded the digitizers, due to unusually large reflectivity of the target. We estimate the actual signal is not very different from the constant level we drew in the figure for t<0.23 μs. The small discontinuity at ~0.32 μs is not associated with the release wave, but due to the shock reaching the rear of the LiF window. (As an independent check, the shock transit time across the LiF derived from this is consistent with the measured wave profile amplitude as drawn.) We have no explanation why the release wave did not appear in the measured profile. The release wave also did not appear in profile R_{yz}. The lack of sufficient reflected light caused the signal beyond 0.4 μs to be untrustworthy.

Sound speed for wet rock

In Fig. 5 the arrows near ~0.5 μs mark the arrival of the release wave, used to calculate the sound speed in the shocked rock. The sound speed versus shock pressure is plotted in Fig. 8.

Series-I wave profiles

Measured and calculated wave profiles for the semi-dry rock are shown in Fig. 9. Again, the complex dynamics of the shock compression of tuff are manifested in the structure of the front of the profile. Note that the lowest pressure shots for the semi-dry and wet tuff, R_e and R_h (Fig. 5) both have an initial 70 - 77 ns rise in their profiles. We believe this is a thick shock front due to pore crushing. The thickness of the front for the semi-dry material R_e, $\Delta t\ U_s$ = 0.24 mm is close to the 0.26 mm value found for the wet tuff R_h.

The lack of a plateau in shots R_e, R_d is due to an unexpectedly high sound speed, which overtook the shock before it reached the Mg/LiF interface, or perhaps to mechanical relaxation phenomena. In shot R_d, the release wave overtakes the shock nearly simultaneous with its arrival at the Mg/LiF interface, so it will have an insignificant effect on the shock transit time. For shot R_e the actual U_s may be slightly higher than the transit time indicates because of overtaking of the shock by the release inside of the rock.

Shots R_g and R_b where shot with the same impactor velocity but using rock from different elevations. The difference in profiles can be ascribed to different behavior of the rock.

In shot profile R_b, the initial step-then-rise could be interpreted as a muddied two-wave structure, similar to that seen in phase transformations under shock loading[6,7]. If the profile is analyzed using this hypothesis we find the transition onset datum shown in Fig. 10a, labeled "Tran". This datum lies on the best fit line for shots R_e and R_d, which is consistent with the existence of a minimum pressure for transformation. The phase transformation hypothesis would explain the softening of the U_s-U_p relation for U_p>~2.1.

Since this phase transformation is very shallow, it is easily overdriven. This would explain why no two-wave structure is seen in the higher pressure shot R_c. The fact that it is not seen in shot R_g could be that the transformation pressure for 1500 ft. rock is just above the pressure achieved by that shot.

The calculated profiles in Fig. 9 were computed from target parameters listed in Tables A.IV and A.V, the U_s-U_p relations indicated in Fig. 3, and gruneisen gamma values from Table IV. Best agreement between measured and calculated curves is with the highest pressure shot. For the lower pressure shots the measured release wave appears sooner than what the gruneisen model predicts, even with the negative gamma values used. For shots R_b and R_g, the target parameters and impactor velocities are so similar that the calculated curve models both.

Sound speed for semi-dry rock

The sound speed in the semi-dry rock was calculated from the arrival of the release wave and plotted in Fig. 8. The sound speed could not be determined for

Table IV. Gruneisen gamma and its slope used in calculated wave profiles for the semi-dry rock. Gamma is linearly dependent on volume. V_1 is the shock pressure.

shot simulated	$\gamma(V_1)$	$V_0(\partial\gamma/\partial V)$	V_1/V_0
R_e	-2	25	0.628
R_d	-2	25	0.588
R_b / R_g	-3	0	0.543
R_c	-3	0	0.453

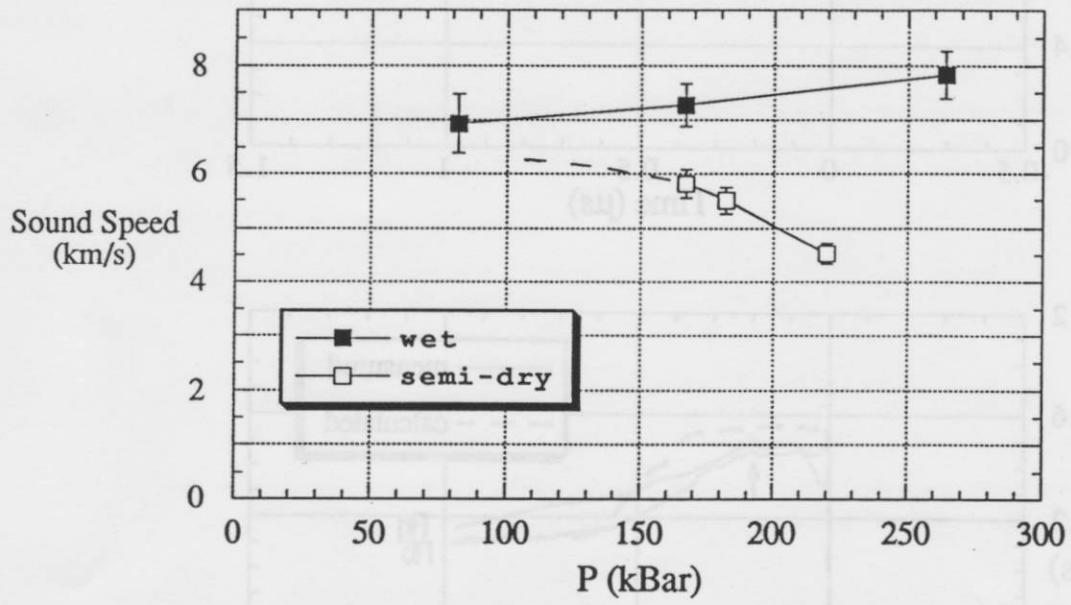

Fig. 8 **Sound speed in the material versus pressure for wet and semi-dry samples.** For the semi-dry material, the lack of a definitive release wave signature in the wave profiles of shots R_e (63 kBar) and R_d (94 kBar) prevents a sound speed determination for them. We believe this is due to a sound speed of 6 km/s or above at 100 kbar overtaking the shock.

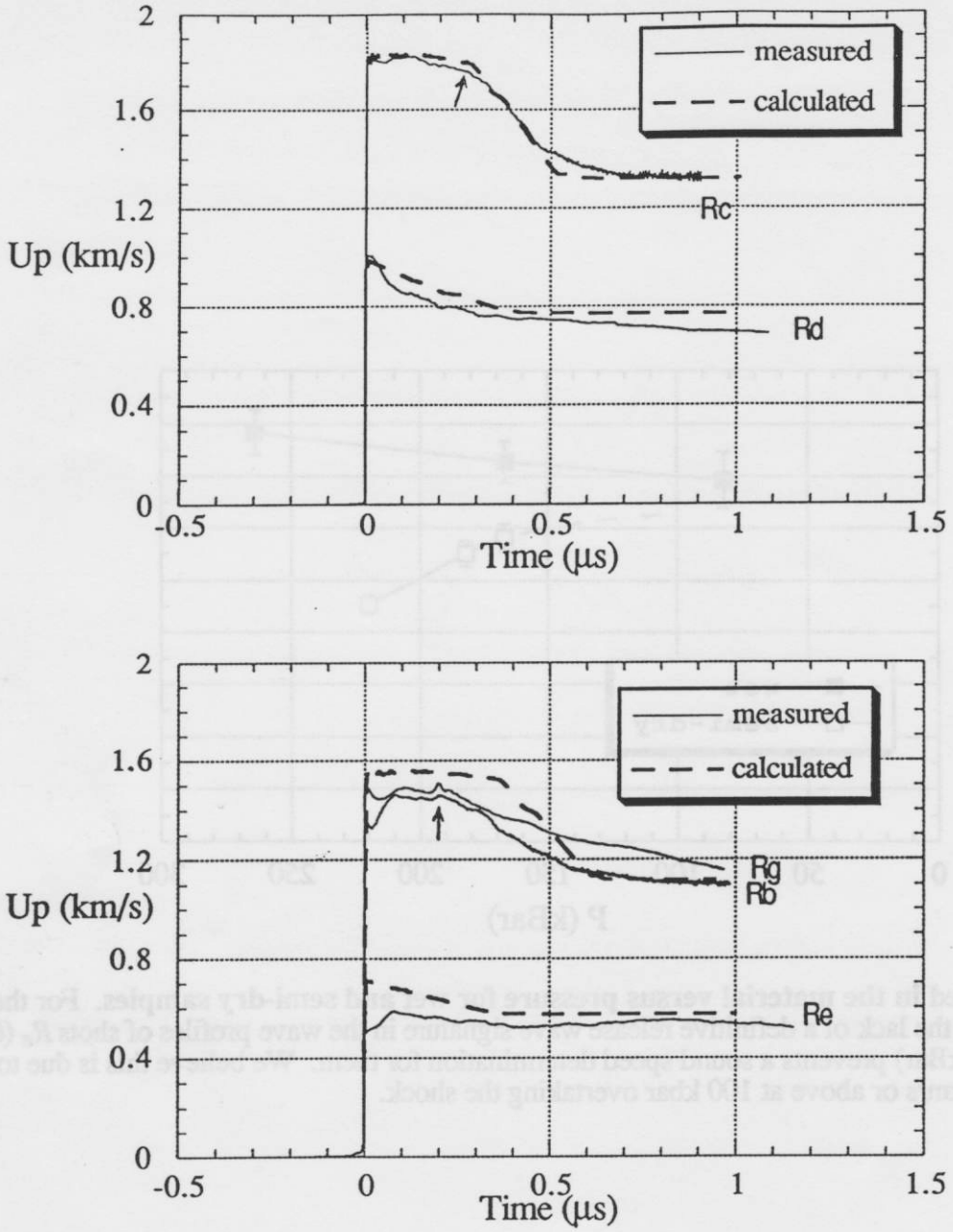

Fig. 9 **Measured and calculated wave profiles for the semi-dry rock.** Arrows indicate when the release wave was taken to arrive at Mg/LiF interface for the sound speed calculation. It appears that the release wave has overtaken the shock in shots R_e and R_d. Shots R_g and R_b had identical impactor velocities but used rock from different elevations– R_g is from 1500 ft., all other from 1410 ft. The calculated curve models both.

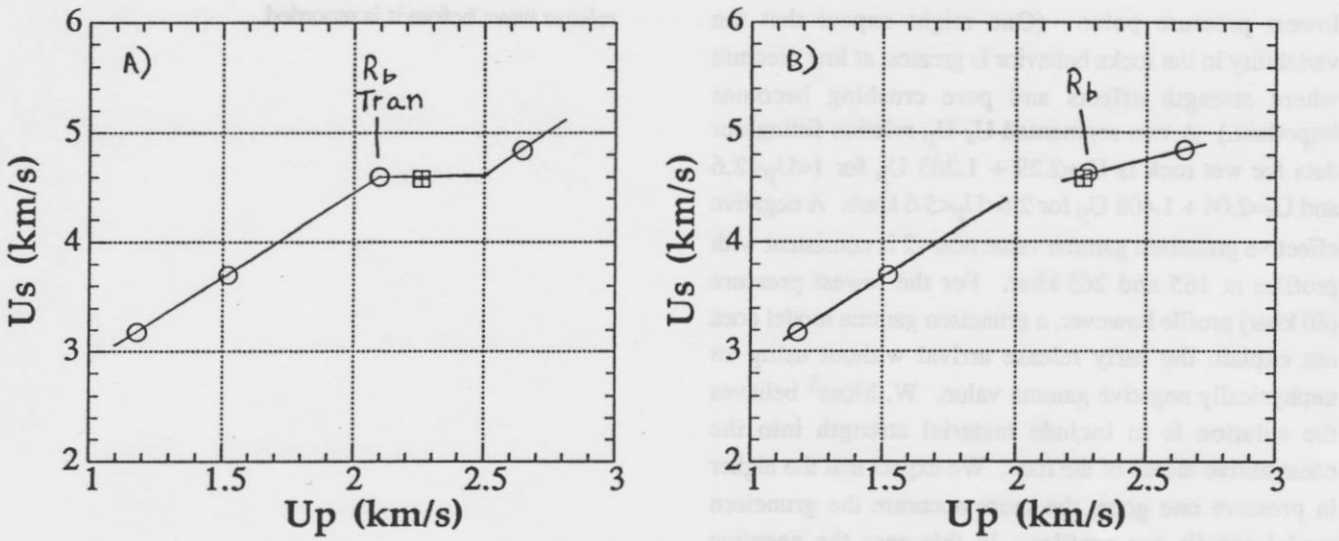

Fig. 10. **Effect on U_s-U_p of interpreting the R_b profile as a two wave structure.** If the first step of the profile of R_b is taken to be the onset of a phase or elastic-plastic transition, then the U_s-U_p has the datum marked "R_b Tran" in part a). If it is taken to be a single wave then the datum is as shown in part b). The rock is 1410 ft. elevation, except for the square datum which is 1500 ft.

the two low pressure shots because the shock has been overtaken by the release wave. If we assume for shot R_d that the release overtakes the shock just as they both reach the Mg/LiF interface, then the sound speed at 94 kbar is above 6 km/s. This suggest that the sound speed versus pressure curve extends as the dashed curve in the Figure.

Conclusions

The U_s-U_p relation for the wet rock agrees very well with M. Furnish's data on similar tuff, except for the lowest pressure point. (One might expect that the variability in the rocks behavior is greatest at low pressure where strength effects and pore crushing becomes important.) A two-segmented U_s-U_p relation fitting our data for wet rock is U_s=2.29 + 1.263 U_p for $1<U_p<2.6$ and U_s=2.04 + 1.408 U_p for $2.6<U_p<5.6$ km/s. A negative effective gruneisen gamma value near -2 is consistent with profiles at 165 and 265 kbar. For the lowest pressure (80 kbar) profile however, a gruneisen gamma model does not explain the early release arrival without using an unphysically negative gamma value. W. Moss[5] believes the solution is to include material strength into the constituitive model of the rock. We expect that the higher in pressure one goes, the more accurate the gruneisen model can fit our profiles. In this case the negative effective gamma might indicate some type of phase transformation.

As the hydration level of this rock is raised, the U_s-U_p relation also rises, and the sound speed at high pressures increases greatly. Whereas for semi-dry rock the sound speed steeply decreases with increasing pressure, for wet rock the sound speed is much higher and slowly increases. In semi-dry rock we see evidence in the U_s-U_p relation and in the wave profile of a possible weak phase transition at ~180 kbar. The was no evidence of such in the wet rock. The significant differences in the shock behavior of the same rock at different hydration states is a compelling reason to accurately preserve in situ conditions in laboratory shock experiments. It also stresses the need to accurately determine the hydration state of in situ rock with elevation along the emplacement hole for subsequent CORRTEX modeling.

It is interesting that in the low pressure (60 - 80 kbar) shots, for both the wet and semi-dry tuff, the wave profile demonstrates complex behavior in the shock compression of rock that is anomalous, or different from what we expect for a simple isotropic material such as aluminum, for example. In both cases, the wave profiles begin with a 70 - 77 ns rise tentatively attributed to a macroscopic shock front 0.24 - 0.26 mm thick due to pore crushing. One important advantage of the forward target geometry is that such information contained in the leading edge of the shock can be obtained clearly. In the reverse target geometry such information would be obscured, since in that design the shock must reflect from the rear of the rock and travel a second time through the sample as a release wave before it is recorded.

APPENDIX

Physical Analysis of rock samples

Table A.I shows the results of physical analysis by TerraTek Inc.[2] of rock taken from different elevations along the emplacement hole.

Target Design

Tables A.II - A.V list the thicknesses and densities of the layers comprising the targets. Comparison of the target thicknesses before and after assembly indicates that a small gap filled with water exists between the rock and either the baseplate or backplate. This gap is due to the bowing of the baseplate and the irregularities of the rock face. (The process of machining the thin baseplate left it slightly bowed). Because the thickness of the water gap is small, the effect on shock propagation is insignificant. However, its effect was included in the analysis of the data and calculated wave profiles by assuming it to be between the baseplate and the sample.

Ultrasound measurements

Ultrasound measurements were done on 1410 ft. rock in both its semi-dry and wet conditions in order determine the sensitivity of the bulk sound speed (C_b) to hydration. In addition to finding that C_b increases with hydration as expected, the results also demonstrated that the variability of the rock from specimen to specimen can be very high. Three samples were cut from the same piece of 1410 ft. rock, and tested with ultrasound in both their dry and rehydrated conditions. The semi-dry condition was achieved by leaving it out in the open air overnight. The rehydrated condition was achieved by soaking it in water overnight. Fig. A1 shows that although the density change is consistent, there is quite a variability in the change in C_b from specimen to specimen. The lack of a significant change in C_b in specimen "Charlie" leads us to distrust the measurement for that specimen.

Table A.I Physical property measurements for material from U4AV emplacement hole.

Depth Interval (ft)	Density			Water by Wet Weight (%)	Porosity (%)	Saturation (%)	Calc Air Voids (%)
	As-Rec'd (gm/cc)	Dry (gm/cc)	Grain (gm/cc)				
1102	2.287	2.128	*	*	*	*	*
1222	1.606	1.277	2.414	20.5	47.1	70.0	14.1
	1.660	1.323	2.389	20.3	44.6	75.7	10.8
Average	1.633	1.300	2.402	20.4	45.9	72.7	12.5
1259	1.758	1.364	2.406	22.4	43.3	91.2	3.8
	1.782	1.415	2.403	20.6	41.1	89.4	4.4
Average	1.770	1.390	2.405	21.5	42.2	90.2	4.1
1368	1.660	1.279	2.365	22.9	45.9	83.2	7.7
	1.668	1.275	2.367	23.8	46.3	85.9	6.5
Average	1.664	1.271	2.366	23.4	46.1	84.5	7.1
1410	1.884	1.564	2.381	17.0	34.3	93.4	2.2
1435	1.566	1.191	2.358	23.9	49.5	75.9	11.9
	1.601	1.221	2.369	23.7	48.5	78.5	10.4
Average	1.584	1.206	2.364	23.8	49.0	77.3	11.1
1445	1.889	1.552	2.534	17.8	38.7	87.3	4.9
	1.923	1.600	2.504	16.8	36.1	89.6	3.8
Average	1.906	1.576	2.519	17.3	37.4	88.3	4.4
1500	1.898	1.589	2.305	16.3	31.1	99.5	0.5
	1.844	1.530	2.470	17.0	38.1	82.6	6.7
Average	1.871	1.560	2.388	16.6	34.7	89.9	3.5

* Grain density measurement compromised during testing by loss of material.

Table A.II. Flyer and target layer thicknesses for the rehydrated shots. The sample diameter was 39 mm, except for shots *Rwx* and *Ryz* where it was 19 mm.

shot	Cu flyer thk (mm)	baseplate thk (mm)	water thk (mm)	rock thk (mm)	Mg thk (mm)	LiF thk (mm)
R_h	3.995	1.444	0.122	6.560	1.031	7.088
R_i	3.894	1.456	0.147	6.340	1.024	7.095
R_j	3.898	1.443	0.115	6.114	1.023	7.093
R_{wx}	2.506	0.987	0.005	3.566	0.979	7.565
R_{yz}	1.989	0.991	0.005	3.506	0.999	8.548

Table A.III. Flyer and target densities for the rehydrated shots.

shot	Cu flyer ρ (gm/cm^3)	baseplate ρ (gm/cm^3)	rock ρ (gm/cm^3)	Mg ρ (gm/cm^3)	LiF ρ (gm/cm^3)
R_h	8.940	8.940	1.851	1.778	2.642
R_i	8.939	8.940	1.854	1.778	2.642
R_j	8.941	8.940	1.852	1.778	2.642
R_{wx}	8.938	8.335	1.903	1.778	2.645
R_{yz}	8.930	8.939	1.903	1.778	2.645

Table A.IV. Flyer and target layer thicknesses for semi–dry samples. The sample diameter was 39 mm.

shot	Cu flyer thk (mm)	rock thk (mm)	Mg thk (mm)	LiF thk (mm)
R_e	2.760	7.013	1.037	7.094
R_d	2.755	7.065	1.036	7.094
R_b	2.752	6.951	1.035	7.090
R_c	2.744	7.024	1.032	7.104
R_g	2.743	7.122	1.040	7.101

Table A.V. Flyer and target densities for semi–dry samples.

shot	Cu flyer ρ (gm/cm^3)	rock ρ (gm/cm^3)	Mg ρ (gm/cm^3)	LiF ρ (gm/cm^3)
R_e	8.939	1.676	1.779	2.642
R_d	8.940	1.676	1.779	2.642
R_b	8.939	1.727	1.779	2.642
R_c	8.939	1.719	1.779	2.642
R_g	8.940	1.756	1.779	2.642

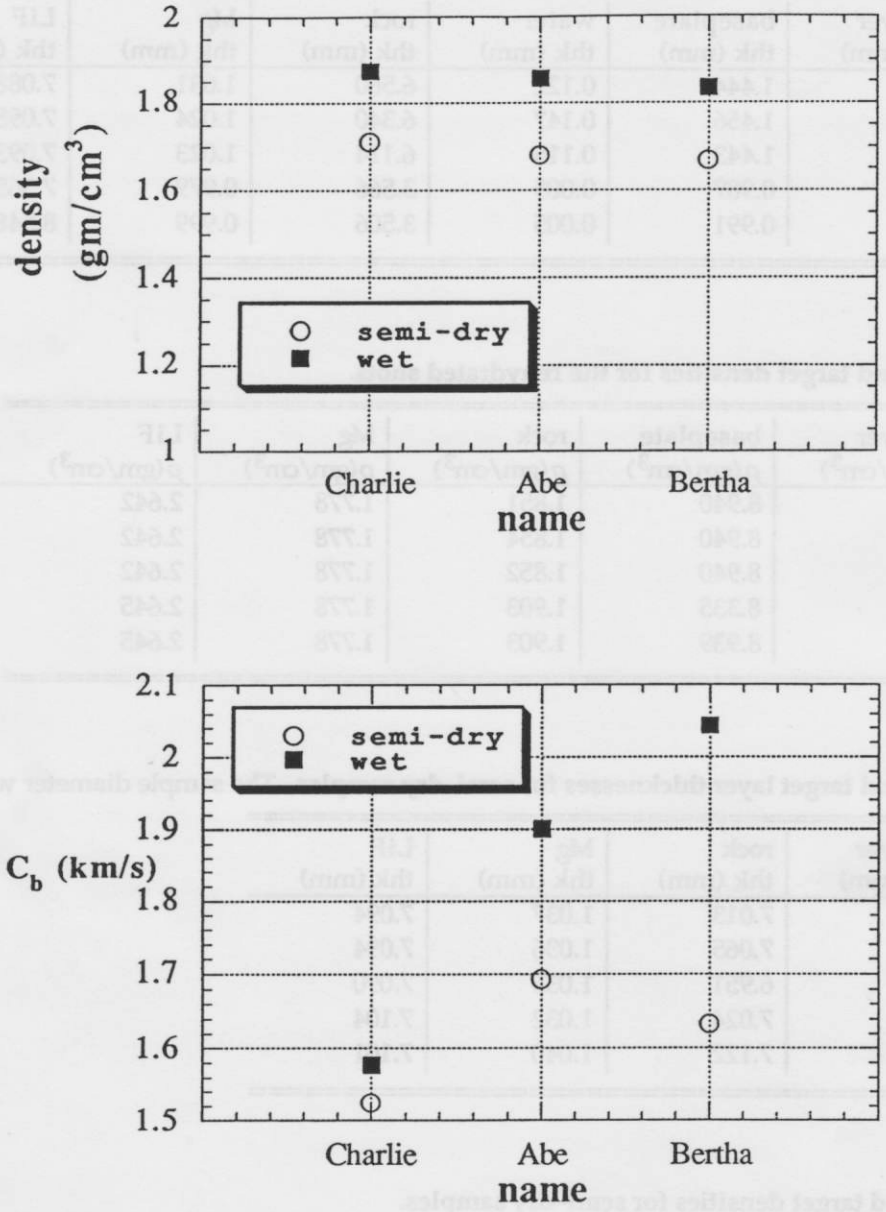

Fig. A1. **The effect of rehydration on ultrasonic sound speed.** The density, transverse (C_t) and longitudinal (C_l) sound speeds were measured via ultrasound on three pieces of 1410 ft. rock in both their semi-dry and rehydrated states. The bulk sound speed C_b was computed from C_t and C_l.

References

1. "*Measuring the dynamic compression and Release Behavior of the Paintbrush and Tunnel Bed (NTS) Tuffs Over the Range 1-13 GPa*", Michael Furnish, Sandia Report SAND90-1317 (1990).
2. TerraTek Inc., 420 Wakara Way, Salt Lake, UT 801-584-2400.
3. W. F. Hemsing, Rev. Sci. Instrum. 50, 73-78 (1979).
4. Sam Weir, LLNL, personal communication (1991).
5. William Moss, private communication, Lawrence Livermore Nat. Lab. (1991).
6. D. J. Erskine and W. J. Nellis, Nature 349, 317 (1991).
7. Ya. B. Zeldovich & Y. P. Raizer, *Physics of Shock Waves and High-Temperature Hydrodynamic Phenomena*, 750-756 (Academic Press, New York, 1967).